Catalysis Today 432 (2024) 114572

Contents lists available at ScienceDirect

Catalysis Today

journal homepage: www.elsevier.com/locate/cattod

Highly efficient carbon catalysts for the green synthesis of 1,5-benzodiazepines: Experimental and theoretical study

Marina Godino-Ojer [a,*], Vanessa Ripoll-Morales [b], Luisa M. Pastrana-Martínez [c], Sergio Morales-Torres [c], Francisco J. Maldonado-Hódar [c], Elena Pérez-Mayoral [d,*]

[a] Facultad de Ciencias Experimentales, Universidad Francisco de Vitoria, UFV, Ctra. Pozuelo-Majadahonda km 1.800, Pozuelo de Alarcón, Madrid 28223, Spain
[b] Departamento de Ingeniería Mecánica, Química y Diseño Industrial, Escuela Técnica Superior de Ingeniería y Diseño Industrial, Universidad Politécnica de Madrid, Ronda de Valencia 3, Madrid 28012 , Spain
[c] NanoTech – Nanomaterials and Sustainable Chemicals Technologies, Departamento de Química Inorgánica, Facultad de Ciencias, Universidad de Granada, Avenida de Fuente Nueva, Granada 18071, Spain
[d] Departamento de Química Inorgánica y Química Técnica, Facultad de Ciencias, Universidad Nacional de Educación a Distancia, UNED, Urbanización Monte Rozas, Avenida Esparta s/n, Ctra. de Las Rozas al Escorial Km 5, Las Rozas-Madrid 28232, Spain

ARTICLE INFO

Keywords:
Acid carbon-based catalysts
Green synthesis
Benzodiazepines
Theoretical calculations

ABSTRACT

A family of sustainable carbon catalysts with different chemical surface, active and selective for the synthesis of benzodiazepine **1** (BDZ), from *o*-phenylendiamine (OPD) **2** and acetone **3**, under mild conditions, is reported. Catalysts were prepared by acids treatments with H_2SO_4 or H_3PO_4 of an activated carbon doped with ZnO at 3% wt (N3Zn) and, subsequently, submitted to additional thermal treatment in air. Simultaneously to the ZnO leaching, surface C-SO_3 groups were generated by treatment of N3Zn with H_2SO_4 (N3Zn-S) whereas treatment with H_3PO_4 led to C-PO_3 functions (N3Zn-P sample). The thermal treatment partially removes the C-SO_3 groups (N3Zn-S-C sample) while C-PO_3 functions were partially oxidized to C-OPO_3 groups (N3Zn-P-C). Our results suggest that these chemical surface modifications of the catalysts are key on catalytic performance, pointed out the importance of the nature and distribution of acid sites at the surface. Remarkably, investigated carbon catalysts (N3Zn-S samples) were more active than the NS catalyst obtained by direct treatment of AC with H_2SO_4, this last mainly functionalized with C-OSO_3 groups. Although the catalysts resulting of the H_3PO_4 treatment showed both a similar activity, some differences on selectivity to BDZ **1** were observed, attributed to certain specificity of P-functions at the surface depending on the acid strength of active sites and the reaction conditions. These results were supported by DFT calculations.

1. Introduction

Under the Green Chemistry principles, prevention of pollution, minimization of the use of solvents and replacement of stoichiometric reagents with catalytic cycles are desirable to develop sustainable, cleaner and safer pharmaceutical processes [1]. In this sense, Green Chemistry could represent a key tool for achieving Sustainable Development Goals (SDGs), such as clean water and sanitation (SDG 6), responsible consumption and production of resources (SDG 12), and actions against climate change (SDG 13) [2].

Carbon-based materials represent a family of promising catalysts in terms of sustainability and energy efficiency for a greener future. Current trends are focused onto the establishment of structure-activity relationships in addition to the identification of active catalytic sites as well as the mechanisms understanding, all of them of capital importance for a future catalyst design. Among the most popular carbon-based materials are the activated carbons (ACs), highly versatile from a point of view of their applications derived from their high surface area, chemical and thermal stability, and long-term performance. In addition, it is widely recognized that the chemical surface, porosity, and pore size distribution of a catalyst play a crucial role controlling both conversion and selectivity. In this context, we recently reported different series of carbon-based catalysts active in the green and selective synthesis of *N*-containing heterocycles such as quinolines, quinoxalines and benzodiazepines all of them compounds of pharmaceutical interest [3]. Particularly, 1,5-benzodiazepines are *N*-heterocycles showing extensive

* Corresponding authors.
E-mail addresses: marina.godino@ufv.es (M. Godino-Ojer), eperez@ccia.uned.es (E. Pérez-Mayoral).

https://doi.org/10.1016/j.cattod.2024.114572
Received 8 November 2023; Received in revised form 30 January 2024; Accepted 5 February 2024
Available online 8 February 2024

applications as biological scaffolds in the field of medicine and pharmacology, such as anxiolytic, sedative, hypnotic, muscle relaxant, anti-inflammatory, antiviral and analgesic [4]. In addition, several commercial drugs are derived from benzodiazepine rings, including clobazam, lofendazam, arfendazam, triflubazam, cystathionine, nevirapine, and telenzepine [5].

While numerous synthesis methods have been reported, the most used approach for producing 1,5-benzodiazepines involves the condensation reaction between diamines and carbonyl compounds. Several structurally different solid catalysts have been applied to the synthesis of 1,5-benzodiazepines, such as zeolites [6,7], HMCM-22 [8], SiO_2-supporting acids – $HClO_4$ [9] and H_2SO_4 [10], mesoporous aluminosilicates [11], clays – modified bentonite [12], Zinc montmorillonite [13], Fe-containing intercalated montmorillonites [14] –, nano-γ-Fe_2O_3–SO_3H [15] and Fe-containing microporous nickel phosphate molecular sieves and Fe-containing mesoporous mesophase materials [16], and so on. Much more recently, Godino et al. reported different series of acidic carbon-based catalysts showing different structures, morphologies, and compositions, for the synthesis of benzodiazepines, from *o*-phenylendiamine (OPD) and acetone, under mild conditions, including ACs treated with HNO_3, H_2SO_4 or mixtures of both [17], supported zirconia or sulfated zirconia composites [18], and phosphor-doped carbon catalysts from spent tires [19]. These studies allowed to confirm that both acid sites and porosity of the catalysts influence both conversion and selectivity. The presence of S-derived functions anchored either zirconia or at the carbon surface could be behind the selectivity enhancement, in addition to the high microporosity of ACs modified with different acids, whereas macroporosity of carbons from pyrolysis of spent tires avoided the diffusional restrictions.

The present work aims to explore the catalytic performance of a new family of eco-friendly functionalized carbon materials to synthetize 1,5-benzodiazepines (BDZ), *via* condensation reaction of OPD **2** and acetone **3** under mild and solvent-free conditions (Scheme 1). Based on our previous studies, the goal of this paper is to functionalise the carbon surface by impregnation with Zn precursor salt followed by thermal treatment [20] which is subsequently treated with acids, H_2SO_4 or H_3PO_4, as fast acid-leaching strategy to alter the carbon surface in terms of both composition and texture. In this context, the influence of the chemical and textural characteristics of different carbon materials on the catalytic performance has been investigated. Complementarily, we report on a computational study analysing the transition structures for the final cyclization step by using the most probable and reduced models simulating the catalytic sites.

2. Materials and methods

2.1. Synthesis of catalysts

A series of carbon catalysts were prepared from N3Zn precursor synthetized by following the experimental protocol previously reported by Godino-Ojer et al. [20]. Briefly, commercial AC sample from NORIT Nederland B.V. (Norit RX3, namely hereafter as sample N, 9 g) was impregnated with concentrated aqueous solution of $Zn(NO_3)_2{\cdot}6\ H_2O$ to obtain a metal loading of 3.0% wt. After drying overnight at 110 ºC, the samples were pre-treated for 2 h under a He flow at 350 ºC (N3Zn sample).

Two independent samples of N3Zn were submitted to acidic treatment in such a manner that N3Zn (3 g) was treated with H_2SO_4 or H_3PO_4 solutions (2 M, 30 mL) and the reaction mixture was stirred for 6 h. The solid was filtered, washed with abundant water and dried at 110 ºC for 12 h. Subsequently, the carbon samples (1.5 g) were treated, or not, with air at 300 °C for 3 h.

The catalyst series were denoted as N3Zn, N3Zn-Y and N3Zn-Y-C where Y indicates the acidic treatment (S= H_2SO_4 and P = H_3PO_4), and C the final thermal treatment.

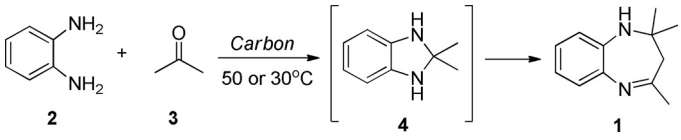

Scheme 1. Synthesis of BDZ **1** from OPD **2** and acetone **3**, at 50 °C, under solvent-free conditions catalyzed by acid carbon materials.

2.2. Characterization of the catalysts

The textural properties of materials were determined from N_2 adsorption–desorption isotherms at – 196 ºC, obtained in a using a Quadrasorb SI equipment (Quantachrome). Before the analysis, all samples were outgassed under high vacuum (10^{-6} mbar) for 8 h at 110 ºC. The apparent surface area (S_{BET}) was determined by applying the Brunauer-Emmett-Teller (BET) equation at $P/P_0 < 0.10$ [21]. The micropore volume (W_0) and the mean micropore width (L_0) were obtained by applying the Dubinin-Raduskevich and Stoeckli equations, respectively [22]. The total pore volume (V_T) was obtained considering the volume of N_2 adsorbed at $P/P_0 = 0.95$ and the mesopore volume (V_{meso}) was obtained from the difference between $V_{0.95}$ and the volume adsorbed at $P/P_0 = 0.40$ by application of the Gurvich rule.

The point of zero charge (pH_{PZC}) of materials was determined following the methodology described elsewhere [23,24]. Solutions were prepared using 25 mL of NaCl (0.01 mol L^{-1}) with HCl (0.1 mol L^{-1}) or NaOH (0.1 mol L^{-1}) to obtain pH values between 2 and 12. Each solution was contacted with 0.10 g of the carbon material and the final pH was measured after 24 h of continuous stirring at room temperature. The final pH was plotted against the initial pH, determining by this way the pH_{PZC}, i.e. the pH value where initial pH = final pH.

X-ray diffraction (XRD) patterns were obtained with a Bruker D8 Discover diffractometer. The surface chemistry of samples was characterized by X-ray photoelectron spectroscopy (XPS) using a Physical Electronic spectrometer (PHI 5701 system) equipped with a Mg 1253.6 eV standard source at 300.0 W and hemispherical electron analyzer.

Elemental analysis of the samples was carried out with an Elemental Analyser LECO CHNS-932. In addition, the zinc amount was determined by Atomic Emission Spectroscopy using an ICP-OES PlasmaQuant PQ 9000 (Analytik Jena) spectrometer.

The morphology of selected carbon-Zn composites was analyzed by high-resolution scanning electron microscopy (HRSEM) with a LEO (Carl Zeiss) GEMINI-1530 microscope.

Amounts of surface acid groups were obtained by titration with bases of different strength (NaOH, Na_2CO_3, and $NaHCO_3$) following Boehm's method [25]. Total surface basicity was obtained by titration with HCl as described elsewhere [26].

Attenuated total reflection Fourier transform infrared (ATR-FTIR) spectra were collected on a Bruker Tensor 27 spectrometer using diamond as ATR crystal (GladiATR, Pike Technologies, Inc.).

2.3. Catalytic performance

To a mixture of OPD **2** (1 mmol) and acetone **3** (10 mmol) in a three-necked vessel, equipped with reflux condenser, septum and thermometer, placed on a multi-experiment workstation StarFish (Radley's Discovery Technologies IUK), at 50 ºC or 30 ºC, the catalyst was added (50 mg) and the reaction mixture was stirred during 240 min. The samples were periodically collected at 15, 30, 60, 120, 180 and 240 min, diluted with acetone (0.5 mL), and the catalyst was filtered off and the solvent evaporated in vacuo.

The catalysts were milled and sieved to particle size < 0.250 mm, in order to avoid mass transfer limitations.

The reaction progress was qualitatively followed by TLC chromatography performed on DC-Aulofolien/Kieselgel 60 F245 (Merk) using

mixtures of CH_2Cl_2/EtOH (98:2) as eluent.

Conversion is defined as the fraction of OPD **2** transformed at each reaction time into compounds determined by ^{1}H NMR.

The reaction products were characterized by ^{1}H NMR spectroscopy. NMR spectra were recorded by using a Bruker AVIII spectrometer (400 MHz for ^{1}H). ^{1}H chemical shifts are referenced to internal tetramethylsilane. Characterization data of benzodiazepine **1** are in good agreement with those previously reported using other catalytic systems [6].

3. Theoretical calculations

Theoretical calculations were performed with the Gaussian 09 software package [27]. Geometries were optimized using RB3LYP/6–31+G (d,p). The stationary points were characterized by means of harmonic vibrational frequency analysis. Thus, the transition structures were confirmed to be first-order saddle points. The imaginary frequency was inspected in each to ensure it represented the desired reaction coordinate. For key transition states, the intrinsic reaction coordinate (IRC) was followed to ensure it connects the reactants and products.

4. Results and discussion

4.1. Characterization of the catalysts

The results obtained by ICP-OES/elemental analysis showed that the N3Zn sample used as reference, presents a bulk Zn loading of 3.1% wt. accordingly with the fitted recipe. After acid treatments the Zn-phase is mainly leached, remaining a Zn content of around 0.5% independently of the acid nature (P or S). However, during these treatments, the introduction of S and P groups simultaneously occurs. The Sulfur and Phosphor contents are around 0.5% and 1.0% wt. respectively.

Table 1 summarized the surface composition of the catalysts determined by XPS. It is noteworthy that the Zn content is higher than the bulk loading, indicating the concentration of this phase on the external surface of the carbon supports. This concentration of metallic particles, basically as ZnO as discussed below, strongly increased the surface oxygen content decreasing the carbon one. The high ZnO surface content also suggests a high dispersion of this phase, because the formation of big crystals will lead to a decrease of the content determined by XPS. Associated to the ZnO phase, the N3Zn catalyst presents a marked basic character, with a pH_{PZC} value of 9.4. As commented previously, the acid treatment clearly induces the Zn leaching. In fact, in spite that ICP analysis showed a certain Zn content, the surface Zn content is negligible in all cases, probably because the rest of Zn could remain in a more internal porosity. Moreover, the results show that the C content increased, and the O content decreased with the leaching of the Zn phase (Table 1). Regarding the formation of S or P-groups, it is noteworthy that the surface P-content (obtained by XPS) clearly fit with the bulk P-content (obtained by ICP), indicating a homogeneous distribution, while the S-groups are predominantly located at surface regarding the bulk. These transformations by leaching and functionalization with P or S also changes the nature of the catalysts surface from basic to acid character.

Fig. 1a-e shows the N_2 adsorption-desorption isotherms of the carbon/ZnO derived catalysts and Table 2 summarizes the textural characterization. The isotherms can be ascribed to type-I, characteristic of microporous materials, in accordance with IUPAC classification [28]. The isotherm profile of all the samples shows a progressive increase of the N_2 adsorbed volume to higher relative pressures and the formation of a hysteresis loop also denoting the formation of mesopores. The deposition of the Zn-phase on the Norit support (sample N3Zn) trigger the partial blockage of the porosity of the Norit ACs. The results show that the S_{BET} decreased in a higher extent than the S_{mic}, probably due to ZnO nanoparticles are mainly located on the external surface (mesopores and large micropores) increasing the mean micropore size (L_0) where N_2-adsorption occurs, also in agreement with the XPS observation.

Table 1
Surface composition (% wt.) determined by XPS.

Sample	pH_{PZC}	C	O	P	S	Zn
		(%)	(%)	(%)	(%)	(%)
N3Zn	9.4	49.6	33.8	0.0	0.0	16.6
N3Zn-P	3.2	90.4	8.6	1.0	0.0	0.0
N3Zn-P-C	3.3	89.3	10.0	0.8	0.0	0.0
N3Zn-S	3.1	88.3	10.4	0.0	1.3	0.0
N3Zn-S-C	3.2	91.2	8.3	0.0	0.5	0.0

After acid treatments (N3Zn-P and N3Zn-S samples) Zn leaching leads to the recovering of porosity, surface values and micropore volume (W_0), but the L_0 values do not change significantly, probably because the remaining rest of Zn (as indicated by ICP) are still blocking the narrowest microporosity. That pore opening also increased with subsequent thermal treatment (N3Zn-P-C and N3Zn-S-C samples), in this case associated to gasification (loss of oxygenated groups, Table 1). Thus, the porosity of samples progressively increased, but never was totally recovered. The micropore widening is maintained because the narrow microporosity remains blocked, leading also to smaller W_0 or V_T regarding the original support.

Fig. 2 displays the XRD patterns of the composites prepared with a metal loading of 3.0% wt. and composites submitted to acidic and thermal treatment. All the XRD patterns exhibit two broad diffraction peaks at around 20° and 45°, which are ascribed to the graphitic (002) and (101) planes, respectively, indicating a certain ordering in amorphous carbon. Overlays to these large bands, the diffractogram of the N3Zn composite shows characteristic peaks of wurtzite hexagonal ZnO nanoparticles (JCPDS 36–1451) although these peaks are too small denoting a lack of crystallinity due to a good ZnO dispersion. The diffraction peaks of ZnO at 31.7°, 34.4°, 36.2°, 47.5°, 56.6°, 62.8°, 66.4°, 67.9°, and 69.0° can be indexed as the (100), (002), (101), (102), (110), (103), (200), (112), and (201) crystal planes. No significant changes on the XRD patterns of the samples after acid/thermal treatments were observed.

Fig. 3a-c shows the deconvoluted O1s, S2p and P2p XPS spectra of the N3Zn, N3Zn-S, N3Zn-S-C, N3Zn-P and N3Zn-P-C and the proportion of the corresponding species identified according to their binding energies are given in Table 3.

The O1s spectrum of N3Zn (Fig. 3a) can be deconvoluted into three components at around 530.7 eV, 532.3 eV and 533.3 eV, corresponding to the O-Zn bonds in the crystal lattice, C═O (either in carbonyl or in carboxyl groups) and C-O (assigned to oxygen in alcohol, ether and epoxy groups, oxygen in carboxyl and/or ester groups) [18]. After acid treatment (N3Zn-S and N3Zn-P samples) the component at 530.7 eV (Zn-O bonds) disappears but a new component at higher binding energy with values of around 536.4 eV, was attributed to P–O or S–O bonds in either phosphate or sulfonic groups, respectively. This component remains even after the subsequent thermal treatment (N3Zn-S-C and N3Zn-P-C samples) although the P- and mainly S-content decrease after this treatment.

The deconvoluted S2p XPS spectra of N3Zn-S and N3Zn-S-C are shown in Fig. 3b. Each S2p peak is the resultant of two components ($2p_{1/2}$ and $2p_{3/2}$) although only the sum of both peaks was plotted in Fig. 3b. The spectra showed the presence of two peaks, namely C-S (~164.1 eV) attributed to S-thiophene-like groups and C–SO_x (~168.3 eV) associated to oxidized forms of sulfur, i.e. sulphonic or even sulphate groups [29, 30]. The predominant S-groups are therefore C-SO_3 (sulphonic groups, Table 3) which slowly decreased after thermal treatment, probably releasing SO_2 with the subsequent decrease of S-content (Table 1). Duran et al. [31] also studied the Norit ACs oxidized with H_2SO_4. They reported a similar S-loading (1.0% wt.) but a different S-group distribution. Thus, although they identify two peaks to fit the S_{2p} region of the XPS spectra, the first one is located at 168.3 eV (0.7% wt.) but the

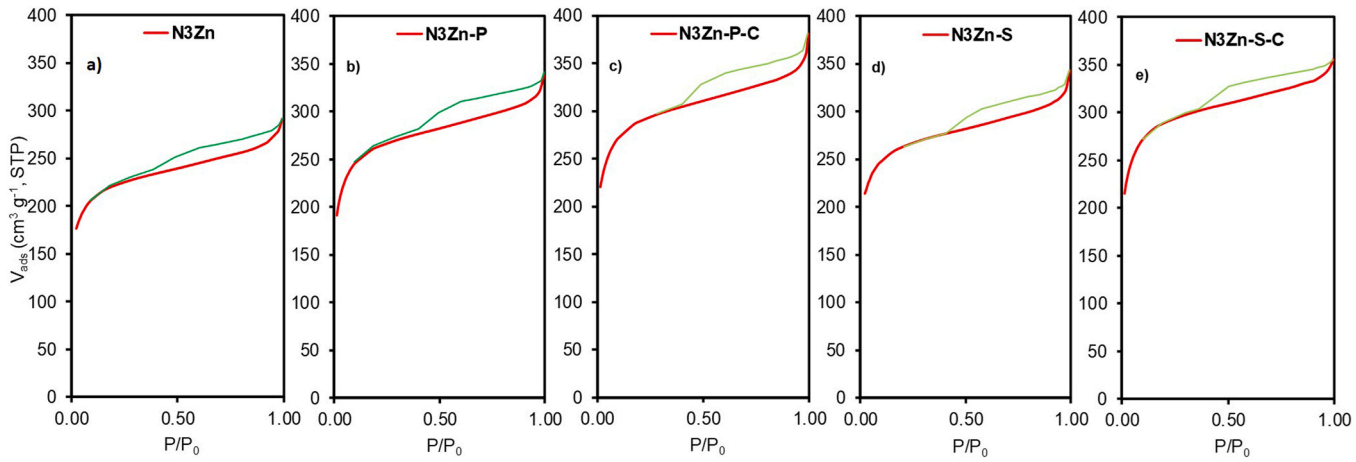

Fig. 1. N_2 adsorption–desorption isotherms at −196°C for investigated carbon materials.

Table 2
Textural parameters of the catalysts.

Sample	S_{BET} (m^2/g)	W_0 (cm^3/g)	L_0 (nm)	S_{mic} (m^2/g)	V_T (cm^3/g)	V_{meso} (cm^3/g)
Norit	1295	0.52	1.3	647	0.61	0.05
N3Zn	840	0.35	1.7	414	0.42	0.05
N3Zn-P	995	0.41	1.6	523	0.49	0.06
N3Zn-P-C	1094	0.46	1.6	565	0.53	0.06
N3Zn-S	993	0.41	1.5	553	0.48	0.06
N3Zn-S-C	1096	0.45	1.6	576	0.52	0.05

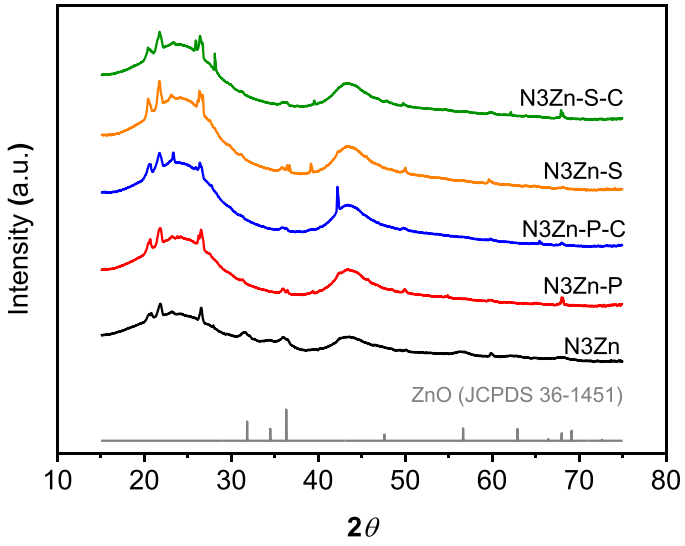

Fig. 2. XRD-patterns of selected carbon-Zn composites.

second one is 169.5 eV (0.3%) associated with sulfate groups. Zhang et al. [32] identify three peaks at 168.6, 167.0, and 167.8 eV (S $2p_{3/2}$) corresponding to –SO_3H, C–SO_2–C, and S–O groups, respectively. Luo et al. [33] describe three sulfur functional groups, including the straight sulfur chain functional group at 163.9 eV, the thiophene functional group at 165.1 eV, and the sulfate functional group at 168.2 eV. The peaks at 164.2 and 169.0 eV are also ascribed to elemental S and sulfates, respectively, as reported elsewhere [34]. Although our results, in agreement with Duran et al. [31], indicate the preferential formation of C-SO_3 groups, the presence of ZnO seems to induce a partial reduction of S-groups, including C-S bonds (as in aromatic structures such as thiophene) or even to elemental S instead the highly oxidized sulfate groups detected by Duran et al. [31].

Regarding the analysis of the P2p region, both N3Zn-P and N3Zn-P-C samples were deconvoluted in two different components, at around 133.5 and 134.8 eV, which correspond to tetrahedral C-PO_3 and C-O-PO_3, respectively (Fig. 3c). Wu et al. [35] reported three bands, the first one centred at around 134.0 eV involving C-O-PO_3 type groups (including i.e. $(CO)_3PO$, $(CO)_2PO_2$ and $(CO)PO_3$), the second one located at 133.4 eV being characteristic of P atom bonded to one or two C atoms and three or two O atoms, as in C–PO_3 or C_2–PO_2 groups. Finally, the band at 132.3 eV was assigned to reduced phosphorus compound as C_3–PO. The latter contribution seems to be negligible in our series of samples. It is noteworthy that phosphor groups are more thermally stable than the sulfur ones showing a smaller removal (Table 1). In fact, these groups are commonly induced to increase the thermal resistance of carbon materials [36]. The peak at 133.5 eV (C-PO_3 groups) are predominantly formed during the acid treatment with H_3PO_4, but they are clearly transformed into C-O-PO_3 groups during thermal treatments in air at 300 °C, in parallel to the increased oxygen content detected after thermal treatment (Table 1) and in contrast with the similar S-sample, where SO_x is released. These results are in agreement with those published by Rosas et al. [36] who described a weight gain of activated carbons doped with P-groups when pretreated in air between 300 and 450 °C, describing the oxidation of C–PO_3 groups into C–OPO_3 as the first step of the oxidation process of ACs treated with phosphoric acid.

The investigated materials have been also characterized by SEM (Fig. 1S) and ATR-FTIR (Fig. 2S). The morphology of the materials consists of heterogeneous and corrugated carbon particles also presenting large pores with a wide range of diameter. Considering the ATR-FTIR spectra of selected carbon-Zn composites, the absorption band located at ca. 1100 cm^{-1} is ascribed to C–O stretching vibration from anhydrides and lactones, the wide band at ca. 1220 cm^{-1} is related with breathing vibrations of epoxy groups (-O-) while the band at ca. 1750 cm^{-1} is characteristic of C═O vibration in carboxylic groups [37, 38]. The peak at ca. 1600 cm^{-1} may be also assigned to skeletal vibrations of graphitic domains (C═C). The bands at ca. 500–600 cm^{-1} could be assigned to vibrational modes of phosphate while both weak bands at ca. 600 and 1090 cm^{-1} could be ascribed to stretching vibrations of C–S and stretching vibrations of S═O, respectively.

It is interesting to note that the intensity of the peak associated to C–O from anhydrides and lactones is significantly higher for the sample treated with phosphoric acid, as previously observed by Boehm titration results (Table 1S).

4.2. Catalytic performance

The performance of carbon catalysts was analyzed using the ZnO-

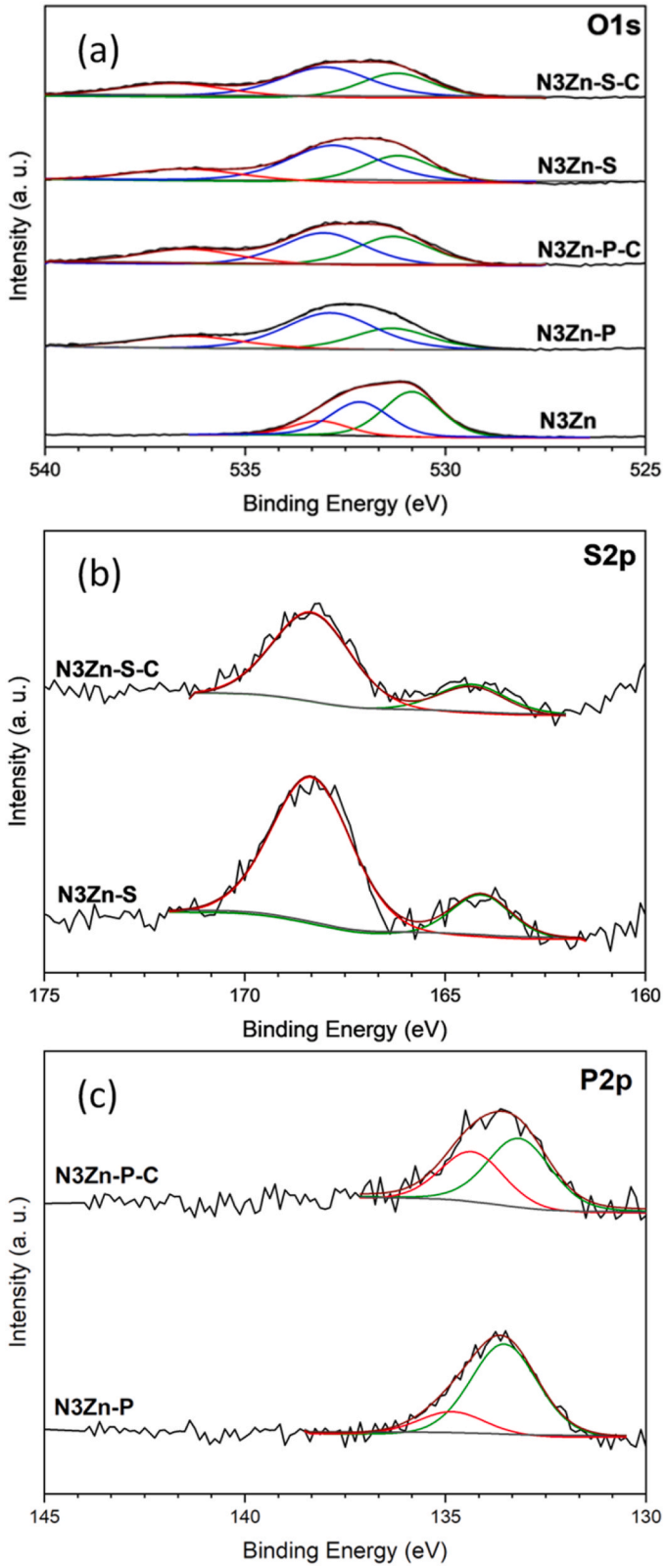

Fig. 3. XPS spectra and fitting of the catalysts: (a) O1s region, (b) S2p region and (c) P2p region.

supported carbon catalyst (N3Zn) and the Norit treated with H_2SO_4 (NS) [17] samples as reference materials. The synthesis of BDZ **1** from OPD **2** and acetone **3**, under solvent-free conditions at different temperatures, according to Scheme 1, was carried out. As it can be seen from Fig. 4a and b, there are significant differences between catalysts regarding both conversion and selectivity values. Sulfuric acid treated catalysts (N3Zn-S and N3Zn-S-C) were active in the reaction reaching high conversion values in comparison with the reference materials. Experiments were carried out at 50 °C using a catalyst amount of 50 mg (except NS experiment, where 100 mg of catalyst was used)). Thus (Fig. 4a), N3Zn-S and N3Zn-P, afforded superior conversion values than N3Zn (more active than typically used ZnO phases), but mainly, specially more active than NS catalysts. The total conversion is also achieved even using 25 mg of catalyst (Fig. 4c). The combination of S-groups generated during acid treatments in presence of ZnO clearly improve those obtained by directly treating the AC support. They also showed a notably increased selectivity values to **1** (Fig. 4b) specially regarding the poor 54% obtained with N3Zn after 2 h. Both catalysts (N3Zn-S and N3Zn-S-C) showed a similar performance (Fig. 4) independently of the weight of catalyst used and the fact of a certain release of S-group after thermal treatments is produced, but the nature of these groups or even the pH_{PZC} values does not change. These results strongly suggest that acid sites at the carbon surface of N3Zn-S and N3Zn-S-C catalysts (pH_{PZC}, Table 1) are behind the observed reactivity and in accordance with results previously reported [17]. Note that for all investigated catalysts compound **4**(scheme 1) was the unique intermediate compound observed.

The performance of phosphoric acid treated catalysts is summarized in Fig. 5. N3Zn-P and N3Zn-P-C catalysts showed similar catalytic performance in terms of conversion (Fig. 5a) or selectivity (Fig. 5b), in spite that the nature of P-groups significantly changes after thermal treatment. Nevertheless, the pH_{PZC} remains similar, and the acidity of both types of P-groups (C-O-PO_3 or C-PO_3) should be strong enough to develop satisfactory this reaction. When compared with N3Zn-S samples, catalysts are also similar regarding the conversion although N3Zn-P showed an enhanced selectivity to **1**, especially in experiments using a low charge of catalyst. In these conditions, N3Zn-P reached, after 1 h of reaction, the highest conversion (95%) and selectivity to **1** (96%) (Fig. 5c, d). When comparing both N3Zn-P and N3Zn-P-C, the former provide higher selectivity values, mainly at short reaction times, although differences are smaller after reaching in both cases the total conversion. This fact suggests a higher specificity of C-PO_3 groups regarding those C-O-PO_3 formed after thermal treatments. Using N3Zn-S and N3Zn-S-C the selectivity increased only increased up to values around 80%, clearly bellow those observed for P-doped ACs, however, in this case, both catalysts show similar selectivity values, because the nature of the active sites remains unchanged after pretreatment. Clearly, reaction is controlled by the nature and distribution of acid sites on the catalyst structure and the subsequent variations that undergoes during treatments. It seems that the catalytic performance is mainly governed by S- or P-derived functions, the contribution of other oxygenated surface groups being neglected (*see* also theoretical calculation section); the concentration of acid and basic sites was measured through the Boehm's method (Table 1S).

Nevertheless, the observed recovering of porosity after the final calcination is unable to improve the performance of acid treated samples.

The influence of the reaction temperature on catalytic performance was also analyzed by decreasing this parameter until 30 ºC. Both conversion and selectivity values decreased for all samples. The performance of samples treated with H_2SO_4 is compared again with the ZnO phase supported on the Norit ACs in Fig. 6. It is noteworthy that N3Zn present in these conditions a performance comparable with N3Zn-S catalyst and clearly superior to N3Zn-S-C, in contrast with the tendency observed at 50 ºC (Fig. 4). Moreover, selectivity showed the contrary tendency, this is, the more active catalysts the smaller selectivity. Thus, N3ZnS-C present selectivity values reaching 90% after 1 h, however, with increasing reaction time and conversion, selectivity decreased again, indicating that the sites producing BDZ **1** are deactivated along reaction. This behavior is not observed for N3Zn-S sample,

Table 3
Species percentages and corresponding binding energies (in brackets, eV) of the materials determined by XPS analysis.

Sample	O1s				S2p		P2p	
	O^{2-}	C═O	C–O	S–O or P–O	C–S	C–SOx	$C–PO_3$	$C–O–PO_3$
N3Zn	49 (530.7)	36 (532.3)	15 (533.3)	-	-	-	-	-
N3Zn-P	-	27 (531.4)	53 (532.9)	20 (536.4)	-	-	80 (133.5)	20 (134.8)
N3Zn-P-C	-	34 (531.3)	43 (533.0)	23 (536.4)	-	-	57 (133.2)	43 (134.3)
N3Zn-S	-	29 (531.2)	49 (532.8)	22 (536.5)	17 (164.1)	83 (168.3)	-	-
N3Zn-S-C	-	31 (531.2)	44 (533.0)	25 (536.8)	21 (164.3)	79 (168.3)	-	-

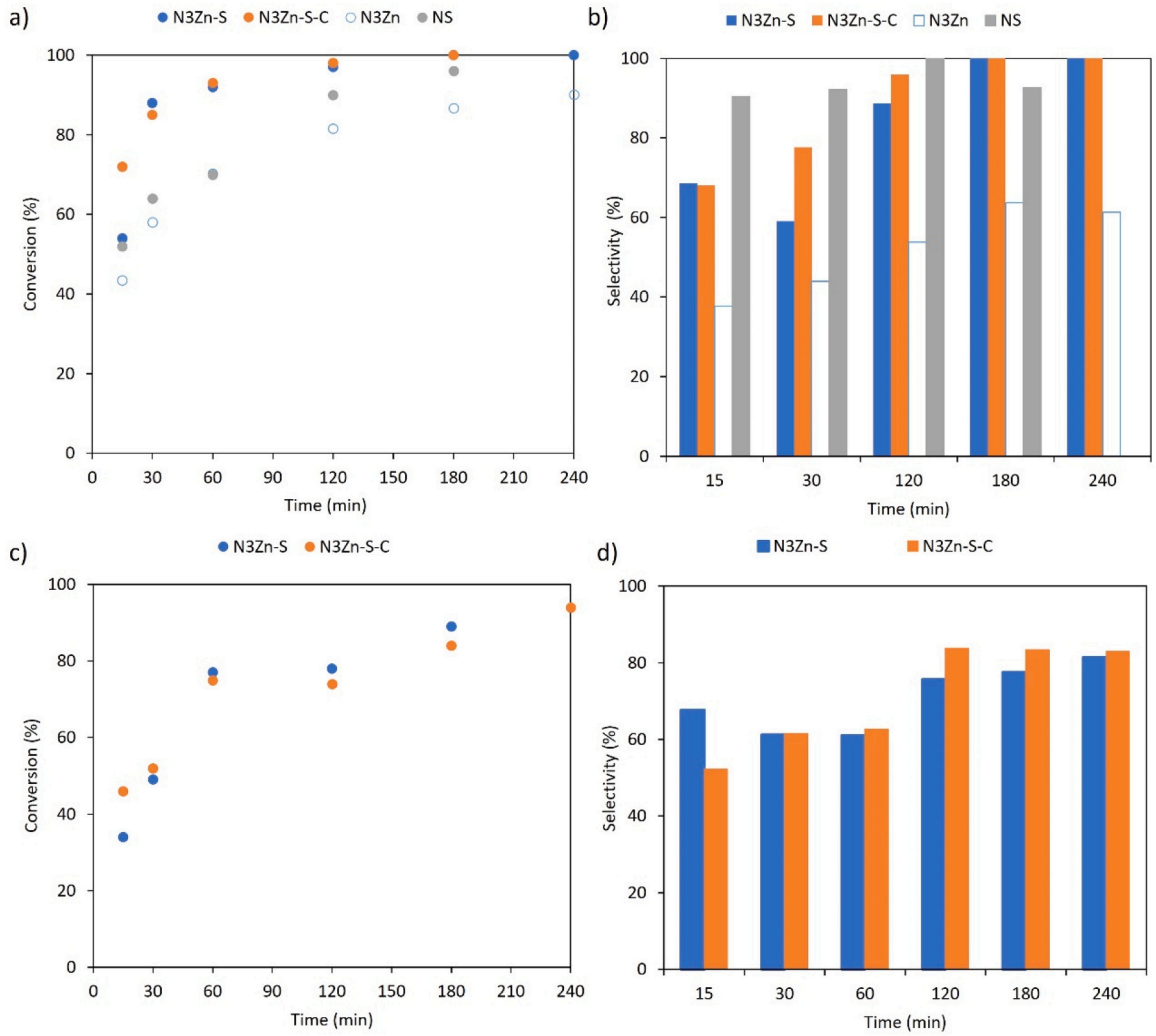

Fig. 4. Synthesis of BDZ **1** from OPD **2** and acetone **3** in the presence of N3Zn-S and N3Zn-S-C catalysts, at 50 °C, under solvent free conditions. Conversion values and selectivity to **1** by using a, b) 50 mg and c, d) 25 mg of each catalyst. NS catalyst (100 mg) [17].

where the concentration of $C-SO_3$ is significantly higher, conversion progressively increased up to total conversion, and the concentration of active sites is enough to maintain more or less constant the selectivity values.

When use P-functionalized catalysts (Fig. 7) a different tendency was observed regarding the performance described for S-treated series. In this case, conversion values of N3Zn-P and N3Zn-P-C are similar, because the most stable P-groups avoid a significant loss of active sites, on the contrary to N3Zn-S. However, the nature of P-groups changes during thermal treatments, thus, in spite that activity is maintained by maintaining the active site concentration Fig. 7b showed how $C-O-PO_3$ groups present on N3Zn-P-C are more selective to **1** than those $C-PO_3$

In summary, all these observations offer valuable mechanistic information useful for future catalyst design. The first imination reaction followed by intramolecular cyclization to **4**, as the unique intermediate compound observed, is mainly favored in the presence of N3Zn catalyst but also when using N3Zn-P catalysts at lower temperature (30 °C). However, the formation of BDZ **1**, as resulted of the final cyclization

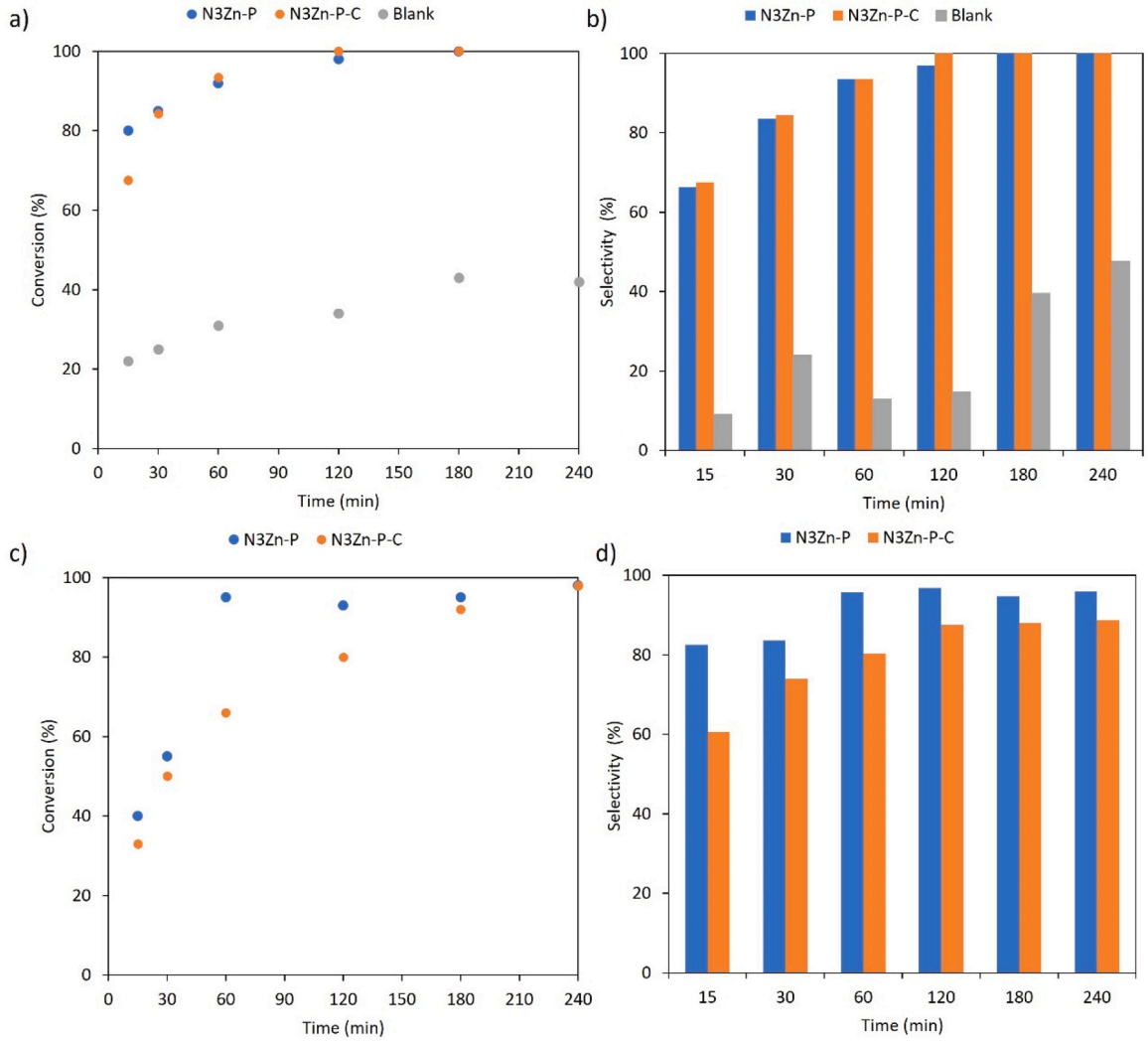

Fig. 5. Synthesis of BDZ **1** from OPD **2** and acetone **3** in the presence of N3Zn-P and N3Zn-P-C catalysts, at 50 ºC, under solvent free conditions. Conversion values and selectivity to **1** by using (a, b) 50 mg and (c, d) 25 mg. Blank experiment was carried out in absence of any catalyst.

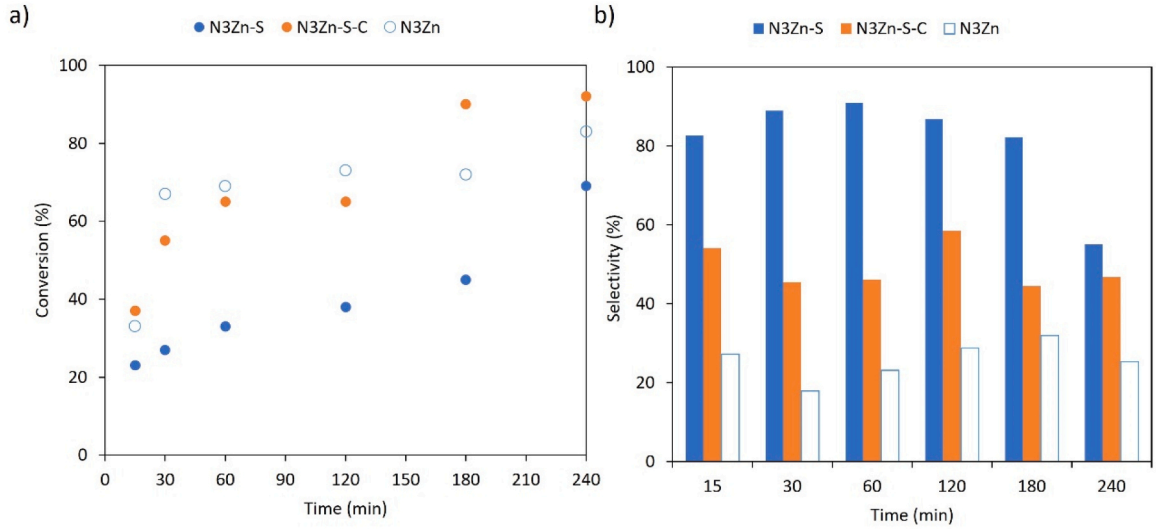

Fig. 6. Synthesis of BDZ **1** from OPD **2** and acetone **3** in the presence of N3Zn-S and N3Zn-S-C catalysts, at 30 °C, under solvent free conditions. a) Conversion values and b) selectivity to **1** by using 50 mg.

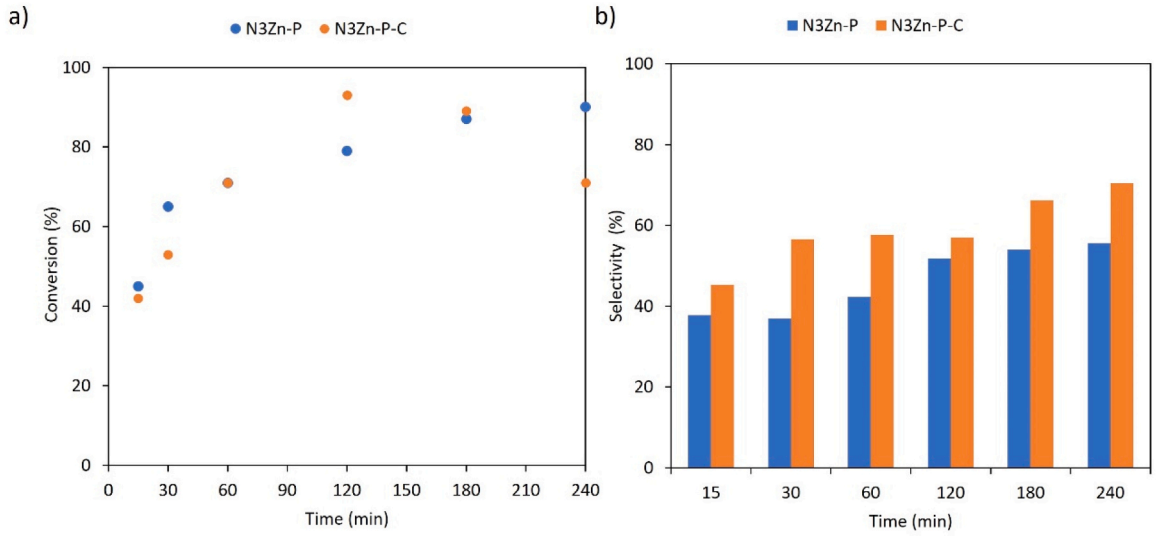

Fig. 7. Synthesis of BZD **1** from OPD **2** and acetone **3** in the presence of N3Zn-P and N3Zn-P-C catalysts, at 30 °C, under solvent free conditions. a) Conversion values and b) selectivity to **1** by using 50 mg.

step, in the presence of N3Zn-S catalyst is strongly favored although in lower conversion. In this case a high selectivity entails a diminished conversion. The obtained results point out that the acid strength of catalytic sites is key in the progress of the reaction from intermediate **4** (Scheme 2) when working at low temperature (30 °C). Then, $-SO_3H$ functions at the carbon surface in N3Zn-S sample are able to catalyze the subsequent steps from the intermediate **4** and particularly the final cyclization step (Scheme 2). In this case the lower conversion values obtained could be attributed to the high adsorption energy of the desired product **1** to these oxygenated groups (*see* computational section). On the contrary, the weak acidity of $-PO_3H_2$ or $-OPO_3H_2$ functions in N3Zn-P samples makes that the formation of benzodiazepine **1** is slower.

In summary, in this work we report on a series of acid carbon catalysts highly efficient in the synthesis of BDZ **1**. Although the formation of S or P-groups on the ACs surface by acid treatments is well known, our results demonstrated the influence of the presence of an active metallic phase (ZnO) during these treatments, which determine the distribution and nature of the generated species. Both acid treatments change the nature of the catalyst from basic to acid in a narrow window of pH_{pzc} values independently of the degree of release of active sites or their transformations after a final calcination treatment. While S-groups are gasified, P-groups change of nature. The concentration and strength of these acid sites determine the performance of the catalysts. Differences are only highlighted under the softer experimental conditions, i.e. low catalysts charge and reaction temperature. In such conditions, it was observed that C-SO_3 groups can be deactivated, while oxidized P-groups, C-O-PO_3 are more selective than those original C-PO_3 ones. Anyway, all these oxygenated groups seem to have the appropriate acid strength to develops the reaction in a similar extent. The conversion values are in general quite similar, except in the case of N3Zn-S-C at soft conditions, where the smaller acid site concentration leads to a smaller conversion values.

In addition, we carried out additional experiment concerning the reuse of the N3ZnP sample, at 50 °C and using 50 mg of the catalyst, after 2 h of reaction time. In this case, the catalyst can be reused during at least two consecutive cycles with both conversion and selectivity maintained (99 and 95% of conversion and 95 and 93% of selectivity). Unfortunately, it was observed a notable decrease of both conversion (37%) and selectivity (62%) after the third cycle, probably due to the interaction of the BDZ **1**, exhibiting basic character, with the acid centers at the catalyst surface. Finally, it was selectively synthetized the corresponding benzodiazepine **1** from OPD **2** and cyclohexanone in 80%, after 4 h of reaction time, in the presence of N3Zn-P catalyst.

4.3. *Theoretical calculations*

In order to rationalize the obtained results, we also carried out a theoretical study concerning the final cyclization step of intermediate **5** (Scheme 2), since this step is key in the selectivity to desired product. Considering the composition at the surface of the investigated carbon-

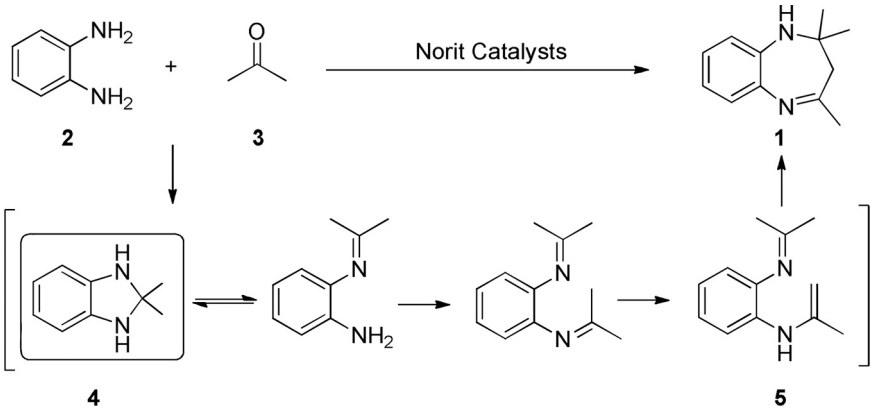

Scheme 2. Reaction mechanism accepted for the synthesis of benzodiazepines.

based catalysts, we selected the models depicted in Fig. 8, which could simulate the acidic catalytic sites at the carbon surface not reflecting the confinement restrictions if any. Considering that the investigated catalysts, particularly N3Zn-S or N3Zn-S-C samples, do not contain C-OSO_3 groups, the Model a was selected for comparison purposes with NS catalyst.

A preliminary inspection of the optimized TS revealed that all the investigated models similarly interact with reagents. This fact seems to be in agreement with the similar conversion behavior observed for the different catalysts in most of the experimental conditions, associated to acid sites with sufficient strength in all cases. Then, the Brönsted acid sites activate the electrophile (imine group in intermediate **5**) promoting the cyclization. Comparing the computed TS, it was observed that while the acidic proton in TS_{OS} (Model a) or TS_S (Model b) is almost totally transferred to the imine group, in the case of TS_{OP} (Model c) or TS_P (Model d) that proton is only partially transferred to electrophile, in accordance with O···H···N═C distances (Table 4), pointing out the relevance of the acid strength of the active sites. Taken into account these observations it could be considered that the acid strength for the selected models could follow the order: $PhOSO_3H$ > $PhSO_3H$ > PhO-PO_3H_2 > $PhPO_3H_2$ in accordance with the pKa values reported for both $PhSO_3H$ and $PhPO_3H_2$ (not found for the others models) i.e. −2.7 and 1.83 (pKa1), respectively (Table 4) [39].

From a thermodynamic point of view, the free-energy values (ΔG) for all optimized TS were significantly lower than that for the TS in absence of any catalyst (Table 4). TS_S and TS_P were the most advanced ones exhibiting the lowest free-energy values. Comparing each type of acid site, the lowest ΔG values correspond to S-derived TS − 34.3 and 24.2 kcal/mol for TS_{OS} and TS_S, respectively −. The same trend was observed for the TS_{OP} and TS_P. Similarly, the activation barrier followed a similar behavior being notably decreased for TS in which S-catalysts are involved.

Considering both the experimental and theoretical results, we can conclude that the surface chemistry is determinant for the observed reactivity, particularly the type and concentration of active sites. Remembering, while N3Zn-S and N3Zn-S-C catalysts presented the same distribution of C−SO_x species (between 79% and 83%) but in smaller concentration by releasing of SO_x, (Table 3), however, the P-content is maintained after calcination, the predominant C−PO_3 groups representing the 80% of the P-groups on N3Zn-P, which were partially transformed into C-O-PO_3 (up to 43% of the P-species) in N3Zn-P-C sample. Comparing the catalytic behavior for N3Zn-S and N3ZnS-C samples, the differences in terms of selectivity to **1** could be due to the high concentration of C−SO_x centers working through the TS_S (Figs. 4, 6 and 9). However, when using the N3Zn-P and N3Zn-P-C samples, which contain similar concentration of P but different distribution of C−PO_3 and C−O−PO_3 sites, the selectivity differences could be attributed to a compromise between the acid strength of active sites and the reaction conditions (Figs. 5, 7, and 9). In spite that the ΔG increased from 30 (TS_P) to 42 kcal/mol (TS_{OP}), it was found that the activation barrier follows the inverse order, being 5.4 Kcal/mol smaller than that for TS_P.

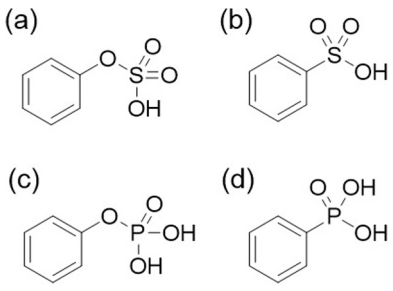

Fig. 8. Reduced models simulating the possible acidic sites tethered at the carbon surface for (a, b) N3Zn-S, (c, d) N3Zn-P catalysts. Models were denoted as (a) OS, (b) S, (c) OP and (d) P as subscript.

Table 4
Optimized TS for the cyclization step to benzodiazepine **1** in the presence of selected models.

TS	TS_{OS} Model a	TS_S Model b	TS_{OP} Model c	TS_P Model d	TS*
O···H···N═C distance (Å)	1.6572	1.6218	1.5816	1.5438	–
C-C distance (Å)	2.2017	2.1895	2.1999	2.1705	1.9940
ΔG (kcal/mol)	34.3	24.2	42.3	30.0	52.1

Note that, in all the cases, it was observed relative strong interactions X═O (X: S or P)···HCH═C (shown in Fig. 9), shortened distances for P-derived TS (TS_{OP} and TS_P), which facilitate the approximation between reagents and catalytic centers. Both interactions condition the advancement of the TS which can be indicative that the acidity of catalytic sites is determinant in the reaction (Fig. 9). Although in all the computed TS the pyramidization of the electrophilic carbon was observed, TS in the absence of any catalyst (not shown) was more advanced than those in the presence of the selected models. The increment of the C-C distances in optimized TS could be mainly due to the interactions with the catalyst presumably more hindered (Table 4.)

* Without catalyst

Remarkably, both samples present similar activity, even at 30 °C, although showing significant differences regarding selectivity to **1**, N3Zn-P-C catalyst being the most selective. This feature reinforces our initial hypothesis concerning the importance of acidity, playing an important role at low temperature. Then, while C-PO_3 functions in N3Zn-P could constitute the active sites working thought TS_P, at 50 °C, C-OPO_3 groups in N3Zn-P-C would be responsible of the enhanced selectivity to **1** at 30 °C, *via* TS_{OP}. In addition, we also computed the optimized TS when using Ph-CO_2H (TS_c not shown), as reduced model simulating the most acidic functions at the carbon surface among the others oxygenated surface groups anchored to the catalyst surface, reaching a ΔG around 1 Kcal/mol lower than TS in absence of any catalyst. It is in good agreement with the experimental results which suggest that the catalytic active sites are mainly S- or P- functions.

On the other hand, it was observed a decreased conversion but increased selectivity to **1** in the presence of N3Zn-S catalyst when the reaction proceeds at 30 °C (Fig. 6). In order to explain this, we analyzed the optimized geometries of BDZ **1** interacting with active sites (Fig. 10).

As an example, the adsorption of BDZ **1** on acid sites is an exothermic process, however, the adsorption on –SO_3H centers (ΔG = −2,3 kcal/mol) is more favored than for –OPO_3H_2 sites (ΔG = −1.2 kcal/mol), these results in accordance with experimental results in terms of conversion and selectivity. This adsorption of the product **1** on the C-SO_3H sites would avoid the desorption of the product at low temperature, which provokes the deactivation of these sites and could justify the selectivity decrease observed at 30 °C with increasing reaction time.

5. Conclusions

We report herein a series of sustainable carbon-based catalysts functionalized with S- or P-oxygenated groups able to efficiently catalyze the synthesis of BDZ **1**, from OPD **2** and acetone **3**, under mild conditions. Catalysts were easily prepared by following a fast acid-leaching strategy from ZnO-supported carbon sample (N3Zn) using H_2SO_4 or H_3PO_4, and subsequent thermal treatment or not, which changes the nature of the catalysts surface from basic to acid character. Interestingly, the H_2SO_4 treatment selectively modified the catalyst surface depending on the carbon precursor. While when using N3Zn sample the selective formation of C-SO_3 functions was observed, the direct H_2SO_4 treatment of AC generated C-O-SO_3 groups.

Catalytic performance is mainly governed by the chemical surface of the catalysts. The treatment of N3Zn with H_2SO_4 produced the modification of the external carbon surface mainly functionalized with C-SO_3 groups (N3Zn-S sample), these groups are partially gasified, leading to lower concentration after the corresponding thermal treatment (surface

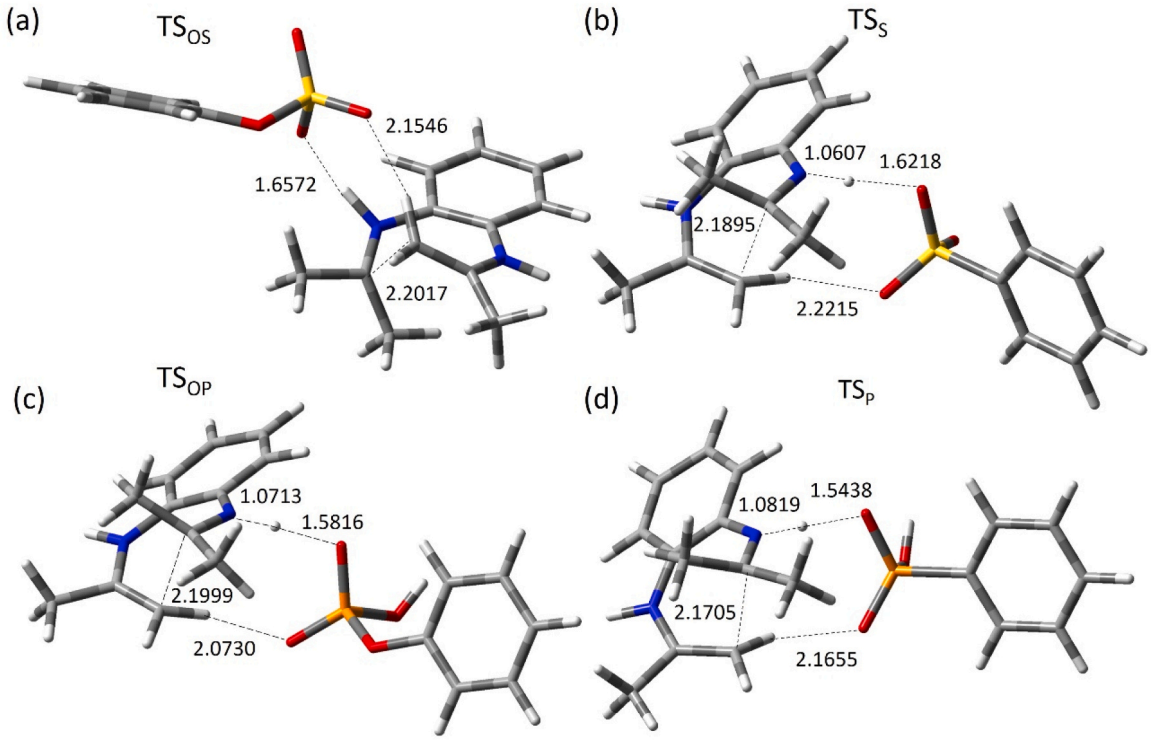

Fig. 9. Optimized TS in the presence of (a, b) N3Zn-S (Models a and b), (c, d) N3Zn-P catalysts (Models c and d) for the cyclization of **5** to **1**. Relevant distances are expressed in Å.

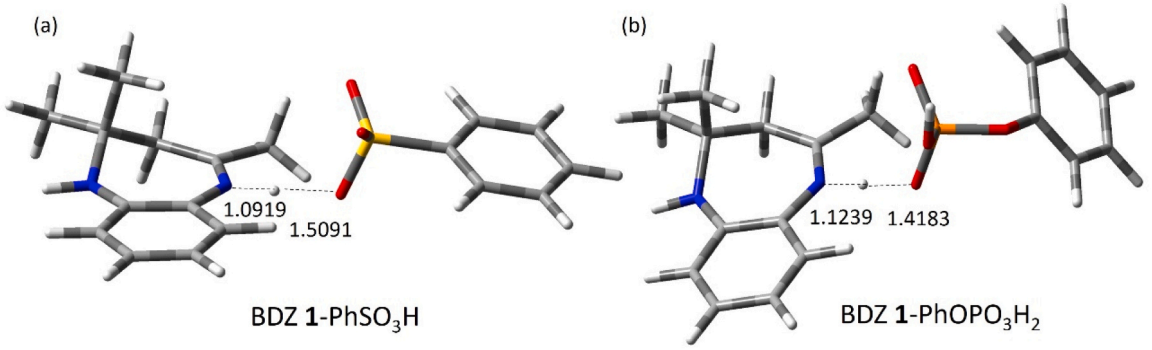

Fig. 10. Optimized geometries comprising the interactions of BDZ **1** with reduced models of active sites. (a) BDZ **1**-Model b and (b) BDZ **1**-Model c. Relevant distances are expressed in Å.

groups -C sample). Treatment with H_3PO_4 generated highly stable C-PO_3 groups (N3Zn-P sample) which are, however, partially oxidized to C-OPO_3 functions during calcination (N3Zn-P sample). Interestingly, these acid carbon catalysts resulted on superior catalytic performance than its precursor (N3Zn), but also the NS sample obtained by direct treatment with H_2SO_4 of commercial Norit AC. The main differences on catalytic performance were observed especially in experiments using either low charge of catalyst (25 *vs* 50 mg at 50 °C) or when working at lower temperature (30 °C *vs* 50ºC). Our results suggest certain specificity of C-O-PO_3 functions in N3Zn-P-C regarding those C-PO_3 groups in N3Zn-P sample, responsible of the increased selectivity. In the case of N3Zn-S and N3Zn-S-C samples, both catalysts reached similar selectivity values due to the unchanged nature of the active sites after the final thermal treatment. In conclusion, the reaction is governed by the nature and distribution of acid sites on the catalysts whereas porosity does not influence the catalytic performance.

In addition, the experimental results are theoretically supported by DFT calculations concerning the final cyclization step to yield BDZ **1**. The optimized TS derived from the most reduced models simulating the active sites for each catalyst suggests that the selectivity differences could be attributed to a compromise between the acid strength of active sites and the reaction conditions.

CRediT authorship contribution statement

Ripoll-Morales Vanessa: Investigation. **Godino-Ojer Marina:** Funding acquisition, Investigation. **Morales-Torres Sergio:** Investigation, Writing – original draft. **Pastrana-Martínez Luisa M.:** Investigation, Writing – original draft. **Pérez-Mayoral Elena:** Conceptualization, Funding acquisition, Supervision, Writing – original draft, Writing – review & editing. **Maldonado-Hódar Francisco J.:** Conceptualization, Funding acquisition, Writing – review & editing, Supervision.

Declaration of Competing Interest

The authors declare that they have no known competing financial

interests or personal relationships that could have appeared to influence the work reported in this paper.

Data Availability

Data will be made available on request.

Acknowledgements

This work has been supported by Universidad Francisco de Vitoria de Madrid (Project Ref. FV2023-38) and by the Projects ref. PID2021-126579OB-C31 and PID2021-126579OB-C32 from MCIN/AEI/10.13039/501100011033 and "ERDF A way of making Europe". S.M.-T. acknowledges to MICIN/AEI/10.13039 /501100011033 and FSE "El FSE invierte en tu futuro" for the Ramon y Cajal research contract.

Appendix A. Supporting information

Supplementary data associated with this article can be found in the online version at doi:10.1016/j.cattod.2024.114572.

References

[1] J. Becker, C. Manske, S. Randl, Green chemistry and sustainability metrics in the pharmaceutical manufacturing sector, Curr. Opin. Green Sustain Chem. 33 (2022) 100562.
[2] T.L. Chen, H. Kim, S.Y. Pan, P.C. Tseng, Y.P. Lin, P.C. Chiang, Implementation of green chemistry principles in circular economy system towards sustainable development goals: Challenges and perspectives, Sci. Total Environ. 716 (2020) 136998.
[3] E. Pérez-Mayoral, M. Godino-Ojer, L.M. Pastrana-Martínez, S. Morales-Torres, F. J. Maldonado-Hódar, Eco-sustainable Synthesis of N-containing Heterocyclic Systems Using Porous Carbon Catalysts, ChemCatChem 15 (2023) 1–23, https://doi.org/10.1002/cctc.202300961, e202300961.
[4] J.B. Bariwal, K.D. Upadhyay, A.T. Manvar, J.C. Trivedi, J.S. Singh, K.S. Jain, A. K. Shah, 1,5-Benzothiazepine, a versatile pharmacophore: a review, Eur. J. Med Chem. 43 (2008) 2279–2290.
[5] S. Teli, P. Teli, S. Soni, N. Sahiba, S. Agarwal, Synthetic aspects of 1,4- and 1,5-benzodiazepines using o-phenylenediamine: a study of past quinquennial, RSC Adv. 13 (2023) 3694–3714.
[6] M. Jeganathan, K. Pitchumani, Solvent-Free Syntheses of 1,5-Benzodiazepines Using HY Zeolite as a Green Solid Acid Catalyst, ACS Sustain, Chem. Eng. 2 (2014) 1169–1176.
[7] M. Firdaus, M. Prameswari, Synthesis of 2,2,4-Trimethyl-2,3-dihydro-1H-1,5-benzodiazepine using Treated Natural Zeolite Catalyst, Bull. Chem. React. Eng. Catal. 14 (2019) 9–16.
[8] S.A. Majid, W.A. Khanday, R. Tomar, Synthesis of 1,5-benzodiazepine and its derivatives by condensation reaction using H-MCM-22 as catalyst, J. Biomed. Biotechnol. 2012 (2012) 510650.
[9] H.M. Meshram, P.N. Reddy, P. Vishnu Murthy, J.S. Yadav, Perchloric acid supported on silica catalyzed efficient synthesis of 1,5-benzodiazepines, Synth. Commun. 37 (2007) 4117–4122.
[10] M.R. Shushizadeh, N. Dalband, SiO2/H2SO4: An efficient catalytic system for solvent-free 1, 5-benzodiazepines synthesis, Jundishapur J. Nat. Pharm. Prod. 7 (2012) 61–64.
[11] D. Shobha, M.A. Chari, S.T. Selvan, H. Oveisi, A. Mano, K. Mukkanti, A. Vinu, Room temperature synthesis of 1,5-benzodiazepine and its derivatives using cage type mesoporous aluminosilicate catalysts, Microporous Mesoporous Mater. 129 (2010) 112–117.
[12] M. Muñoz, G. Sathicq, G. Romanelli, S. Hernández, C.I. Cabello, I.L. Botto, M. Capron, Porous modified bentonite as efficient and selective catalyst in the synthesis of 1,5-benzodiazepines, J. Porous Mater. 20 (2013) 65–73.
[13] R. Varala, R. Enugala, S.R. Adapa, Zinc montmorillonite as a reusable heterogeneous catalyst for the synthesis of 2,3-dihydro-1H-1,5-benzodiazepine derivatives, ARKIVOC 2006 (2006) 171–177.
[14] B. González, R. Trujillano, M.A. Vicente, A. Gil, V.N. Panchenko, E.A. Petrova, M. N. Timofeeva, Two synthesis approaches of Fe-containing intercalated montmorillonites: differences as acid catalysts for the synthesis of 1,5-benzodeazepine from 1,2-phenylenediamine and acetone, Appl. Clay Sci. 146 (2017) 388–396.
[15] A. Amoozadeh, M. Malmir, N. Koukabi, S. Otokesh, Microwave-assisted, solvent free preparation of 1,5-benzodiazepine derivatives using nanomagnetic-supported sulfonic acid as a recyclable and heterogeneous catalyst, J. Chem. Res. 39 (2015) 694–697.
[16] M.N. Timofeeva, S.A. Prikhod'ko, K.N. Makarova, M.E. Malyshev, V.N. Panchenko, A.B. Ayupov, S.H. Jhung, Iron-containing materials as catalysts for the synthesis of 1,5-benzodiazepine from 1,2-phenylenediamine and acetone, React. Kinet. Mech. Catal. 121 (2017) 689–699.
[17] M. Godino-Ojer, I. Matos, M. Bernardo, R. Carvalho, O.S.G.P. Soares, C. Durán-Valle, I.M. Fonseca, E.P. Mayoral, Acidic porous carbons involved in the green and selective synthesis of benzodiazepines, Catal. Today 357 (2020) 64–73.
[18] M. Godino-Ojer, L. Milla-Diez, I. Matos, C.J. Durán-Valle, M. Bernardo, I. M. Fonseca, E. Pérez, Mayoral, enhanced catalytic properties of carbon supported zirconia and sulfated zirconia for the green synthesis of benzodiazepines, ChemCatChem 10 (2018) 5215–5223.
[19] M. Godino-Ojer, V.R. Morales, A.J. López Peinado, M. Bernardo, N. Lapa, A. M. Ferraria, A.M.B. do Rego, I.M. Fonseca, I. Matos, E. Pérez-Mayoral, P-Doped carbon catalyst highly efficient for benzodiazepine synthesis, Tires Valoris., Catal. Today 419 (2023) 114160–114172.
[20] M. Godino-Ojer, S. Morales-Torres, E. Pérez-Mayoral, F.J. Maldonado-Hódar, Enhanced catalytic performance of ZnO/carbon materials in the green synthesis of poly-substituted quinolines, J. Environ. Chem. Eng. 10 (2022) 106879–106888.
[21] S. Brunauer, P.H. Emmett, E. Teller, Adsorption of Gases in Multimolecular Layers, J. Am. Chem. Soc. 60 (1938) 309–319.
[22] R. Haul, S.J. Gregg, K.S.W. Sing: Adsorption, Surface Area and Porosity, second ed., Academic Press, 1982 (Chapter 4), 86 (1982), pp. 957-957.
[23] C.A. Leon y Leon, J.M. Solar, V. Calemma, L.R. Radovic, Evidence for the protonation of basal plane sites on carbon, Carbon 30 (1992) 797–811.
[24] L.M. Pastrana-Martínez, S. Morales-Torres, S.K. Papageorgiou, F.K. Katsaros, G. E. Romanos, J.L. Figueiredo, J.L. Faria, P. Falaras, A.M.T. Silva, Photocatalytic behaviour of nanocarbon–TiO_2 composites and immobilization into hollow fibres, Appl. Catal. B-Environ., 142– 143 (2013) 101–111.
[25] H. Boehm, Advances in Catalysis, vol. 16, Academic Press,, New York, 1966.
[26] C. Moreno-Castilla, F. Carrasco-Marin, E. Utrera-Hidalgo, J. Rivera-Utrilla, Activated carbons as adsorbents of sulfur dioxide in flowing air. Effect of their pore texture and surface basicity, Langmuir 9 (1993) 1378–1383.
[27] M.J. Frisch, G.W. Trucks, H.B. Schlegel, G.E. Scuseria, M.A. Robb, J.R. Cheeseman, G. Scalmani, V. Barone, B. Mennucci, G.A. Petersson, H. Nakatsuji, M. Caricato, H. P.H.X. Li, A.F. Izmaylov, J. Bloino, G. Zheng, J.L. Sonnenberg, M. Had, Gaussian 09, Revision C.01, Gaussian, Inc., Wallingford CT, (2010), pp. (n.d.).
[28] S. Brunauer, L.S. Deming, W.E. Deming, E. Teller, On a Theory of the van der Waals Adsorption of Gases, J. Am. Chem. Soc. 62 (1940) 1723–1732.
[29] S.-A. Wohlgemuth, F. Vilela, M.-M. Titirici, M. Antonietti, A one-pot hydrothermal synthesis of tunable dual heteroatom-doped carbon microspheres, Green. Chem. 14 (2012) 741–749.
[30] J.P. Paraknowitsch, A. Thomas, J. Schmidt, Microporous sulfur-doped carbon from thienyl-based polymer network precursors, Chem. Commun. 47 (2011) 8283–8285.
[31] C.J. Durán-Valle, M. Madrigal-Martínez, M. Martínez-Gallego, I.M. Fonseca, I. Matos, A.M. Botelho do Rego, Activated carbon as a catalyst for the synthesis of N-alkylimidazoles and imidazolium ionic liquids, Catal. Today 187 (2012) 108–114.
[32] B. Zhang, M. Gao, W. Tang, X. Wang, C. Wu, Q. Wang, H. Xie, Reduced surface sulphonic acid concentration Alleviates carbon-based solid acid catalysts deactivation in biodiesel production, Energy 271 (2023) 127079–127090.
[33] J. Luo, C. Zhang, C. Yao, D. Ma, Y. Chen, M. Tian, H. Xie, L. Pan, Y. Zhen, R. Chen, J. Wu, C. Lu, F. Feng, X. Xu, Q. Wang, Q. Zhang, X. Li, Sulfur-doped activated carbon supported platinum species as robust catalysts for nitrobenzene hydrogenation to p-Aminophenol, Mol. Catal. 545 (2023) 113216–113228.
[34] J. Luo, K. Wang, Y. Qian, P. Wang, H. Yuan, O. Sheng, B. Li, H. Wang, Y. Wang, Y. Liu, J. Nai, X. Tao, W. Li, Covalent sulfur confined in mesoporous hollow carbon spheres for effective kinetic regulation of room-temperature sodium-sulfur batteries, Nano Energy 118 (2023) 108958–108968.
[35] X. Wu, L.R. Radovic, Inhibition of catalytic oxidation of carbon/carbon composites by phosphorus, Carbon 44 (2006) 141–151.
[36] J.M. Rosas, R. Ruiz-Rosas, J. Rodríguez-Mirasol, T. Cordero, Kinetic study of the oxidation resistance of phosphorus-containing activated carbons, Carbon 50 (2012) 1523–1537.
[37] L.M. Pastrana-Martínez, S. Morales-Torres, V. Likodimos, P. Falaras, J. L. Figueiredo, J.L. Faria, A.M.T. Silva, Role of oxygen functionalities on the synthesis of photocatalytically active graphene–TiO_2 composites, Appl. Catal. B: Environ. 158–159 (2014) 329–340.
[38] L.M. Pastrana-Martínez, S. Morales-Torres, V. Likodimos, J.L. Figueiredo, J. L. Faria, P. Falaras, A.M.T. Silva, Advanced nanostructured photocatalysts based on reduced graphene oxide-TiO2 composites for degradation of diphenhydramine pharmaceutical and methyl orange dye, Appl. Catal. B-Environ. 123-124 (2012) 241–256.
[39] M. Kim, F. Sanda, T. Endo, Polymerization of Glycidyl Phenyl Ether with Phosphonic Acid Esters as Novel Thermally Latent Initiators, Macromolecules 32 (1999) 8291–8295.